Title	Experimental and numerical characterisation of the elasto-plastic properties of bovine trabecular bone and a trabecular bone analogue
Author(s)	Kelly, Nicola; McGarry, J. Patrick
Publication Date	2012
Publication Information	Kelly, N,McGarry, JP (2012) 'Experimental and numerical characterisation of the elasto-plastic properties of bovine trabecular bone and a trabecular bone analogue'. Journal Of The Mechanical Behavior Of Biomedical Materials, 9 :184-197.
Link to publisher's version	http://dx.doi.org/10.1016/j.jmbbm.2011.11.013
Item record	http://hdl.handle.net/10379/4022
DOI	http://dx.doi.org/http://dx.doi.org/10.1016/j.jmbbm.2011.11.013

Kelly, N. and McGarry, J. P. Experimental and numerical characterisation of the elasto-plastic properties of bovine trabecular bone and a trabecular bone analogue. Journal of the Mechanical Behavior of Biomedical Materials 2012; 9:184-197.

http://dx.doi.org/10.1016/j.jmbbm.2011.11.013

Experimental and Numerical Characterisation of the Elasto-Plastic Properties of Bovine Trabecular Bone and a Trabecular Bone Analogue

Abstract

The inelastic pressure dependent compressive behaviour of bovine trabecular bone is investigated through experimental and computational analysis. Two loading configurations are implemented, uniaxial and confined compression, providing two distinct loading paths in the von Mises-pressure stress plane. Experimental results reveal distinctive yielding followed by a constant nominal stress plateau for both uniaxial and confined compression. Computational simulation of the experimental tests using the Drucker-Prager and Mohr-Coulomb plasticity models fails to capture the confined compression behaviour of trabecular bone. The high pressure developed during confined compression does not result in plastic deformation using these formulations, and a near elastic response is computed. In contrast, the crushable foam plasticity models provide accurate simulation of the confined compression tests, with distinctive yield and plateau behaviour being predicted. The elliptical yield surfaces of the crushable foam formulations in the von Mises-pressure stress plane accurately characterise the plastic behaviour of trabecular bone. Results reveal that the hydrostatic yield stress is equal to the uniaxial yield stress for trabecular bone, demonstrating the importance of accurate characterisation and simulation of the pressure dependent plasticity. It is also demonstrated in this study that a commercially available trabecular bone analogue material, cellular rigid polyurethane foam, exhibits similar pressure dependent yield behaviour, despite having a lower stiffness and strength than trabecular bone. This study provides a novel insight to the pressure dependent yield behaviour of trabecular bone, demonstrating the inadequacy of uniaxial testing alone. For the first time, crushable foam plasticity formulations are implemented for trabecular bone. The enhanced understanding of the inelastic behaviour of trabecular bone established in this study will allow for more realistic simulation of orthopaedic device implantation and failure.

Keywords

Trabecular bone, experimental testing, confined compression, plasticity, pressure dependence yield, polyurethane foam.

Abbreviations

bovine trabecular bone (BTB), polyurethane foam (PU), Drucker Prager (DP), Mohr-Coulomb (MC), isotropic crushable foam (CFI), volumetric crushable foam (CFV), Young's modulus (E), yield stress (σ_y), elastic Poisson's ration (v_e), plastic Poisson's ration (v_p), von Mises equivalent stress (q), equivalent pressure stress (p), von Mises-pressure stress (q-p).

1. Introduction

Trabecular bone is a highly porous cellular structure composed of a complex interconnected network of rods and plates called trabeculae. Its material properties are dependent on many factors including density, age, sex, species, geometry and anatomic site (Goldstein, 1987; Keaveny et al., 1993b; Morgan et al., 2003). Both cellular rigid and solid rigid polyurethane foam (PU), commercially available trabecular bone analogue materials (Sawbones, Pacific Research Labs, Malmö, Sweden), have been widely used as trabecular bone substitutes in biomechanical testing (Agneskirchner et al., 2006; Poukalova et al., 2010; Cawley et al., 2011). A range of rigid closed cell PU foams (grades 5 - 50, ρ = 0.08 - 0.8 g/cm^3) have been identified in ASTM F1839-08 (ASTM, 2008). This artificial bone material has become an attractive alternative over cadaveric bone due to its availability, uniformity, low inter-specimen variability, reproducibility and clean testing environment. It has a similar cellular structure and many of its elastic properties are in the same order of magnitude as trabecular bone (Thompson et al., 2003; Patel et al., 2008). Due to its intricate porous lattice-like structure, the mechanical response of cellular foams and trabecular bone during uniaxial compressive loading are complex. The stress-strain curve of a cellular material typically displays three phase deformation behaviour. An initial linear elastic region occurs due to elastic cell bending which is followed by material yield causing collapse of the cell walls under constant load. An inelastic section follows where a constant stress plateau occurs due to progressive cell wall damage, breakage and buckling under increased loading. A steep stiffness increase called densification occurs when the cell material consolidates due to cells collapsing and contacting (Goldstein, 1987; Szivek et al., 1993; Neilsen et al., 1995; Gibson, 2005). Due to its widespread use as a trabecular bone substitute material for biomechanical applications, grade 20 cellular rigid closed cell PU was used in this study. Additionally, grade 50 solid rigid PU foam is also considered.

Knowledge of the complex deformation behaviour of trabecular bone is important at a clinical and biomechanical level. Previous studies investigating non-linear trabecular bone mechanics have uncovered viscoelastic, damage and elasto-plastic behaviour (Linde, 1994; Keaveny et al., 1999; Moore and Gibson, 2002a). The present study focuses on elasto-plastic behaviour, in particular focusing on the role of pressure (hydrostatic stress) in the yield behaviour of trabecular bone. Inelastic deformation can occur due to excessive loading or fatigue and may lead to microdamage, fracture, compaction and crushing of trabecular bone (Moore and Gibson, 2002b). Inelastic loading also occurs during the subsidence of prostheses, such as vertebral fusion devices, and the implantation of press-fit prostheses in total joint arthroplasty (Taylor et al., 1998; Kelly and McGarry, 2011). As trabecular bone is naturally confined by stiff cortical bone it is reasonable to suggest that high pressures will occur during such inelastic deformation. Despite this, the pressure dependent plastic yielding of trabecular bone has not previously been investigated.

Previous continuum level finite element studies characterising the elasto-plastic behaviour of bone have focused primarily on cortical bone. Several studies have considered von Mises plasticity which neglects pressure dependent yield (Lotz et al., 1991; Keyak and Rossi, 2000; Keyak, 2001; Mullins et al., 2009; Adam and Swain, 2011). Additionally, several studies have focused on the Drucker-Prager (DP) (Mercer et al., 2006; Bessho et al., 2007; Mullins et al., 2009; Carnelli et al., 2010; Adam and Swain, 2011; Carnelli et al., 2011) and Mohr-Coulomb (MC) (Tai et al., 2006; Wang et al., 2008) constitutive formulations. Through the definition of a friction angle the DP and MC models allow for an increasing yield stress for increasing pressure. Comparing the

von Mises and DP models for the simulation of cortical bone nanoindentation, Mullins et al. (2009) suggested that a pressure dependent yield criterion should be used when modelling the post yield behaviour of cortical bone due to frictional mechanisms.

Cortical and trabecular bone have different micro architecture (Keaveny et al., 2001) and therefore the plasticity mechanisms of both materials may be very different. The inelastic behaviour of cellular materials, such as trabecular bone and PU foam, are related to the micro-structural level deformation. At the level of single trabeculae, Wang et al. (2008) used the MC model to simulate nanoindentation. While DP and MC type material behaviour may be appropriate for cortical bone and for individual trabeculae, the suitability of such plasticity models has not previously been investigated for macroscale behaviour of trabecular bone. Inelastic continuum material models have also been proposed that can account for trabecular bone morphology (Zysset and Curnier, 1996; Zysset and Rincon-Kohli, 2006; Rincon-Kohli and Zysset, 2009; Charlebois et al., 2010a). Due to the experimental evidence that at the apparent level trabecular bone yields at a nearly constant strain within an anatomic site (Kopperdahl and Keaveny, 1998; Chang et al., 1999; Morgan and Keaveny, 2001; Bayraktar and Keaveny, 2004), strain-based inelastic material models have been developed and implemented for trabecular bone (Cowin and He, 2005). In contrast, trabecular bone yield stress and elastic modulus are not uniform within anatomic site (Chang et al., 1999; Morgan and Keaveny, 2001). Van Rietbergen et al. (1996,1998) demonstrated that a uniform uniaxial yield strain exists for trabecular bone that is independent of the direction of loading. Micro-architecture based high-resolution FE models have been used to investigate trabecular bone behaviour (Niebur et al., 2000; Niebur et al., 2002; Bayraktar et al., 2004; Harrison et al., 2008; Mc Donnell et al., 2009; Guillén et al., 2011). Detailed reconstruction of the trabecular bone micro-architecture allows for the simulation of non-linear behaviour while using simplified material constitutive laws, however, micro-structural based FE models are of limited use for macroscale simulation of orthopaedic device performance. In contrast, the macroscale inelastic behaviour of trabecular bone can be modelled using continuum constitutive models that are less complex and less computationally expensive than micro-structural based models. Continuum models are investigated in the current study in an attempt to phenomenologically replicate the complex inelastic material behaviour of trabecular bone and may potentially be applied to macroscale trabecular bone applications involving inelastic deformation.

The current study involves a detailed experimental and numerical investigation of the elasto-plastic macroscale behaviour of PU and bovine trabecular bone (BTB). Both uniaxial and confined compression tests are performed in order to identify two distinct loading paths on the von Mises-pressure stress (q-p) plane. The main aim of the study is to investigate, for the first time, the pressure dependent yield behaviour of trabecular bone under confined compression and to determine a constitutive formulation that best captures this behaviour. Due to widespread use of cellular and solid rigid PU foams as trabecular bone analogues for biomechanical testing our secondary aim is to compare the pressure dependent plasticity of such foams to that of trabecular bone. The following pressure dependent constitutive formulations are investigated: DP; MC; isotropic crushable foam (CFI); volumetric crushable foam (CFV).

2. Materials and methods

2.1 Experimental

Cubic specimens of 8 mm of grade 20 cellular rigid closed cell PU foam (ρ = 0.32 g/cm^3) and grade 50 solid rigid closed cell PU foam (ρ = 0.80 g/cm3, E = 1148 MPa, ~9.99 % closed cell) by Sawbones (Pacific Research Labs, Malmö, Sweden) and BTB were cut using a bandsaw (Jubilee VBS 360, Addison Saws Ltd., West Midlands, UK). For the remainder of this document the grade 20 cellular rigid PU will be referred to as "cellular PU" and the grade 50 solid rigid PU will be referred to as "solid PU". It should be noted that only one density of each foam type has been tested and therefore the results apply only to these particular density foams. The BTB specimens were prepared from the proximal tibia of a bovine steer under 30 months obtained from a local abattoir and stored at 4°C prior to testing. BTB specimens were kept hydrated in phosphate buffer solution (PBS) with the marrow *in situ* at all times, including during mechanical testing, and were tested with their principal trabecular orientation approximately aligned parallel to the axis of loading. BTB was chosen for the experimental study over cadaveric bone due to the size and availability of specimens and its similarity to human trabecular bone.

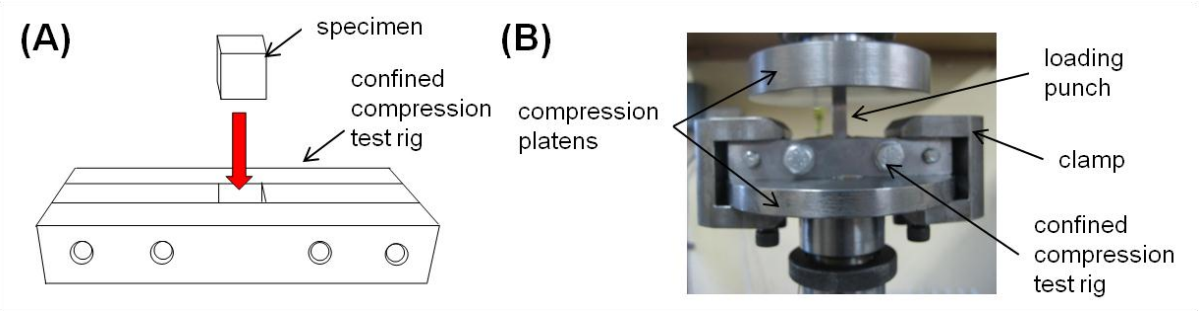

Fig. 1 - (A) Schematic of experimental rig used for confined compression testing. (B) Confined compression experimental set-up on an Instron testing machine.

Plano-parallel specimen ends were produced using sandpaper. The PU and BTB specimen dimensions were taken as an average of four measurements with a digital vernier calliper before testing to account for the inhomogeneity of the samples and were randomly assigned to experimental groups. Two different loading configurations were investigated; uniaxial compression and confined compression. Compression is a dominant *in-vivo* loading mode for trabecular bone and confined compression is appropriate as trabecular bone is typically confined by a hard cortical shell. Destructive static compression tests were performed on the cellular PU and BTB at room temperature on a servo hydraulic testing machine (Model 8500, Instron Corp., Canton, MA, USA) equipped with a 100 kN load cell (n = 9/group). 36 tests were performed in total; nine specimens were tested for the each specimen type (cellular PU and BTB) and for each test configuration (uniaxial and confined). Uniaxial compression was performed using the conventional platens test and the specimens were placed between polished parallel hardened steel platens. The confined compression tests were performed on a custom made confinement rig (Fig. 1) which prevented lateral displacement of the specimen during loading. The test specimens were placed in a hole in the rig which was the same size as the specimens. The rig was then secured between the two loading platens using clamps, as shown in Fig. 1(B). A loading punch with a cross-sectional area of 8 x 8 mm was used to load the specimen via the compression platens. For both uniaxial and confined compression testing, a 5 - 10 N compressive preload was applied and the specimens were loaded at a constant

strain rate of 5 mm/min to 60 % strain. Air exposure was kept to a minimum during BTB testing. Additional uniaxial (n = 5) and confined (n = 5) compression testing was also performed on the solid PU to elucidate any pressure dependent behaviour of the ~99.9 % closed cell foam. Preliminary uniaxial compression testing was performed on five cellular PU specimens in each of the three loading directions (n = 15 in total). Two sample t-tests were performed to determine statistical significance between the three uniaxial loading directions. Significance was determined at $p<0.05$.

Nominal stress-nominal strain curves were constructed based on undeformed specimen dimensions. The apparent compressive Young's modulus (E) was computed as the slope of the uniaxial nominal stress-nominal strain curve between 30 % and 70 % of the ultimate stress (Turner, 1989; Keaveny et al., 1993b;1993a). The yield stress (σ_y) was determined using the 0.2 % offset method. The elastic Poisson's ratio (v_e) and plastic Poisson's ratio (v_p) were measured using a video extensometer (ME 46, Messphysik, Fürstenfeld, Austria).

2.2 Material model calibration

Finite element simulations (Abaqus v6.8 Dassault Systemes, RI, USA) were performed in order to establish suitable elasto-plastic constitutive formulations for both PU and BTB. Both materials were both treated as a homogenous continuum and modelled using each of the aforementioned elasto-plastic material models: DP; MC; CFI; CFV. Using 3D continuum elements, boundary conditions were applied to replicate the uniaxial and confined compression experimental tests. Both the PU and BTB were compressed to 60 % strain. Each of the elasto-plastic material models was used in combination with an isotropic, linear elastic material model where a value of E and v_e were required. A hardening curve, describing the uniaxial compressive yield stress as a function of the corresponding plastic strain, determined from the mean uniaxial experimental nominal stress-nominal strain curve for PU and BTB, were used to describe the inelastic behaviour. Material parameter calibration was conducted for each constitutive model to identify an accurate numerical solution for the experimental results under uniaxial compression. Following model calibration under uniaxial compression, parameter variation under confined compression was simulated in order to investigate the pressure dependent plastic behaviour of each material model. The computed response was compared to experimental confined compression data. The yield surface and flow potential of all four constitutive models considered in the study are governed by the von Mises equivalent stress (q) and the equivalent pressure stress (p) where

$$q = \sqrt{\frac{3}{2}(S:S)} \qquad p = -\frac{1}{3}trace(\sigma)$$

And S is the stress deviator.

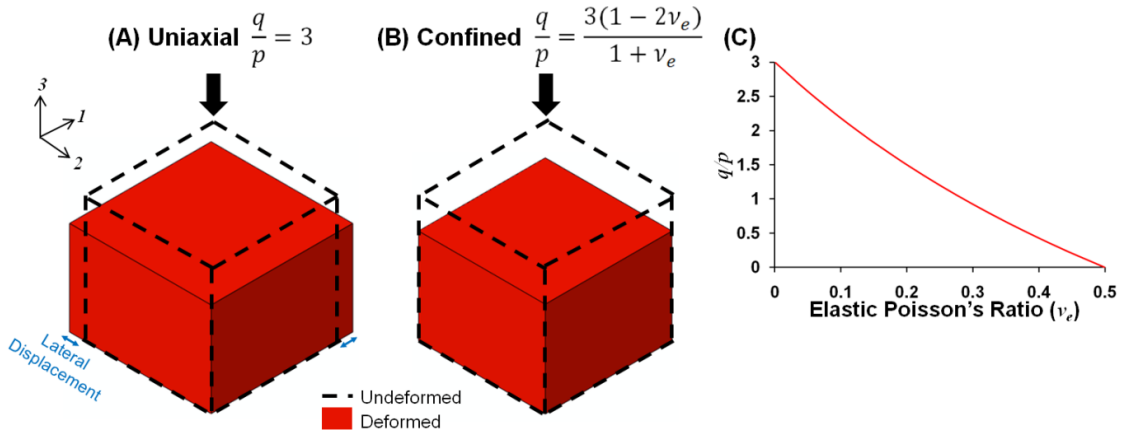

Fig. 2 - (A) Schematic of uniaxial compression for an elastic Poisson's ratio, ν_e, of 0.3. (B) Schematic of confined compression. (C) Relationship between the ratio *q/p* (von Mises stress/pressure stress) and the elastic Poisson's ratio (ν_e) for confined compression of an isotropic elastic material.

The stress state in uniaxial compression (Fig. 2(A)) is expressed in terms of a single principal stress component in the loading direction (σ_{33}). It therefore follows that $q/p = 3$ for uniaxial tests, independent of ν_e. In confined compression three principal stress components exist (σ_{11}, σ_{22}, σ_{33}) when load is applied axially (direction *3*), and lateral deformation of the specimens is prevented in the other two directions (whereby $\varepsilon_{11} = \varepsilon_{22} = 0$, $\sigma_{11} = \sigma_{22}$) (Fig. 2(B)). Using Hooke's law for an isotropic elastic material, it is trivial to determine the ratio of von Mises stress to pressure as a function of ν_e (Fig. 2(B,C)). As an illustrative example, for a $\nu_e = 0.3$, $q/p = 0.92$ for a confined compression test. Therefore, by performing both uniaxial and confined compression tests up to yielding in tandem, two distinct points on a yield surface in the *q-p* plane can be established as shown in Fig. 3. Examples of the yield surface calibration of a DP or MC type material and a crushable foam type material are shown in Fig. 3Fig. (B,C).

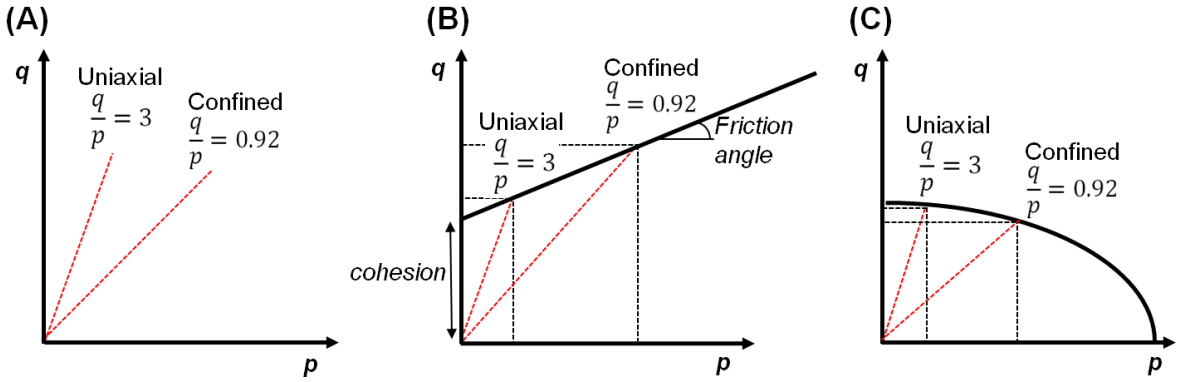

Fig. 3 - (A) Schematic of the loading path for uniaxial compression and confined compression for an elastic material in the *q-p* plane; (B) Schematic of a Drucker-Prager or Mohr-Coulomb type yield surface; (C) Schematic of a crushable foam type yield surface. *q* = von Mises stress, *p* = pressure.

The DP and MC plasticity models are very similar; their yield surfaces are represented by a straight line the *q-p* plane (Fig. 3(B)). The DP criterion was introduced by Drucker and Prager (1951) and was traditionally used to model soils. Both the DP and MC models have previously been calibrated for cortical bone (Mercer et al., 2006; Tai et al., 2006; Mullins et al., 2009), where a high friction angle results in an increased von Mises yield stress with increasing pressure as shown in Fig. 3(B). Refer to the appendix for further information on the yield criterion and flow rule for the DP and MC formulations.

Crushable foam plasticity models can phenomenologically represent the buckling of cell walls under compression of a cellular material. The crushable foam yield surface is an ellipse in the *q*-*p* plane (Fig. 3(C), Fig. 4). An increase in pressure leads to a lower von Mises stress at yield for the CFI and CFV models, in contrast to DP and MC plasticity. The CFI model is based on a model by Deshpande and Fleck (2000). It assumes symmetric behaviour in tension and compression and the yield ellipse is centred at the origin of the *q*-*p* plane (Fig. 4(A)).

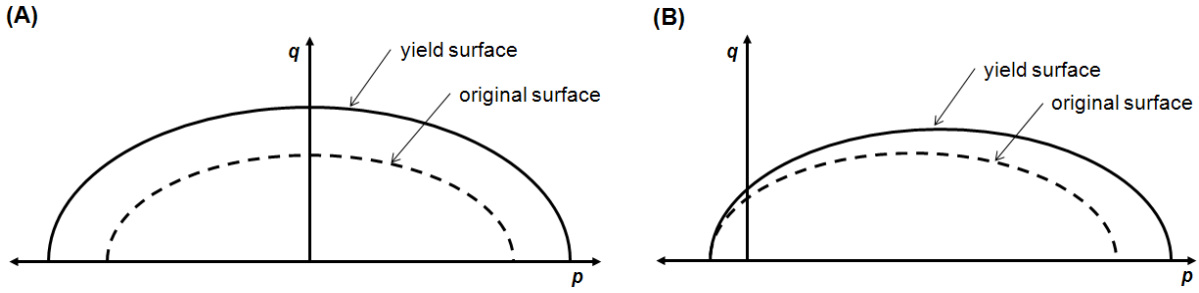

Fig. 4 – The yield surface and yield surface evolution for: (A) CFI model; (B) CFV model.

The yield criterion for the CFI model is given by:

$$F = \sqrt{q^2 + \alpha^2 p^2} - B = 0 \qquad B = \alpha p_c \qquad \alpha = \frac{3K}{\sqrt{9-K^2}} \qquad K = \frac{\sigma_c^0}{p_c^0}$$

The flow potential for the CFI model is given by:

$$G = \sqrt{q^2 + \beta^2 p^2} \qquad \beta = \frac{3}{\sqrt{2}}\sqrt{\frac{1-2\upsilon_p}{1+\upsilon_p}}$$

Where α is the shape of the yield ellipse in the *q*-*p* stress plane, B is the size of the yield ellipse, p_c is the yield strength in hydrostatic compression, K is the compression yield stress ratio, σ_c^0 is the initial yield strength in uniaxial compression, p_c^0 is the initial yield strength in hydrostatic compression, β is the ellipse for the potential flow and υ_p is the plastic Poisson's ratio. The yield ellipse progression is governed by the equivalent plastic strain (Deshpande and Fleck, 2000). In contrast to the CFI model, the CFV model allows for asymmetric compression-tension behaviour. The CFV yield ellipse is not centred at the origin and during plastic deformation the hydrostatic tension strength is assumed fixed (Fig. 4(B)). The yield stress in uniaxial compression evolves due to an increase (compaction) or decrease (dilation) in material density. The yield criterion for the CFV foam model is given by:

$$F = \sqrt{q^2 + \alpha^2 (p - p_0)^2} - B = 0 \qquad \alpha = \frac{3K}{\sqrt{(3K_t+K)(3-K)}} \qquad K = \frac{\sigma_c^0}{p_c^0} \qquad K_t = \frac{p_t}{p_c^0}$$

The flow potential for the CFV model is given by:

$$G = \sqrt{q^2 + \frac{9^2}{2}\, p^2}$$

Where p_o is the centre of the yield ellipse, K_t is the hydrostatic yield stress ratio and p_t is the yield strength in hydrostatic tension. The CFV yield ellipse progression is governed by the volumetric compacting plastic strain. Given the large deformations that occur during mechanical testing, with plastic strains exceeding 50 %, finite

deformation kinematics was implemented in all models. However, for convenience, both experimental and computational results are plotted in terms of nominal stress and nominal strain.

3. Results

3.1 Experimental

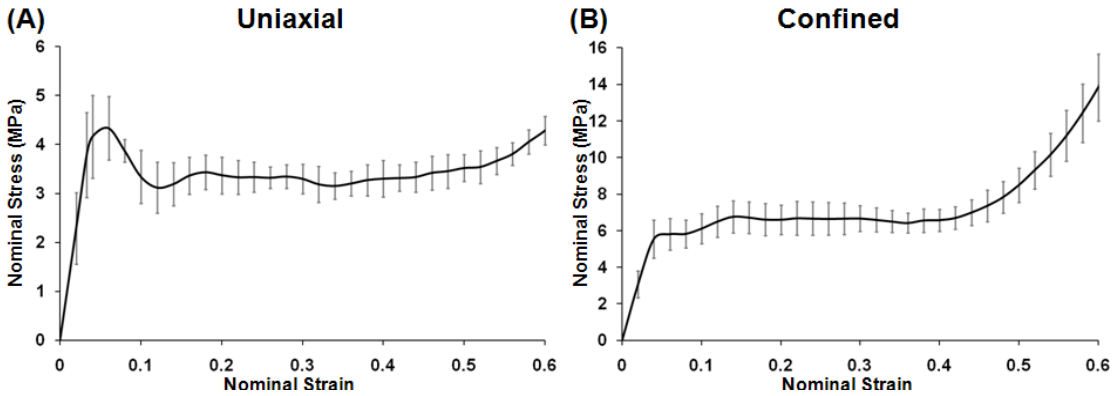

Fig. 5 - Grade 20 cellular rigid polyurethane foam experimental results: (A) mean ± SD for uniaxial compression; (B) mean ± SD for confined compression.

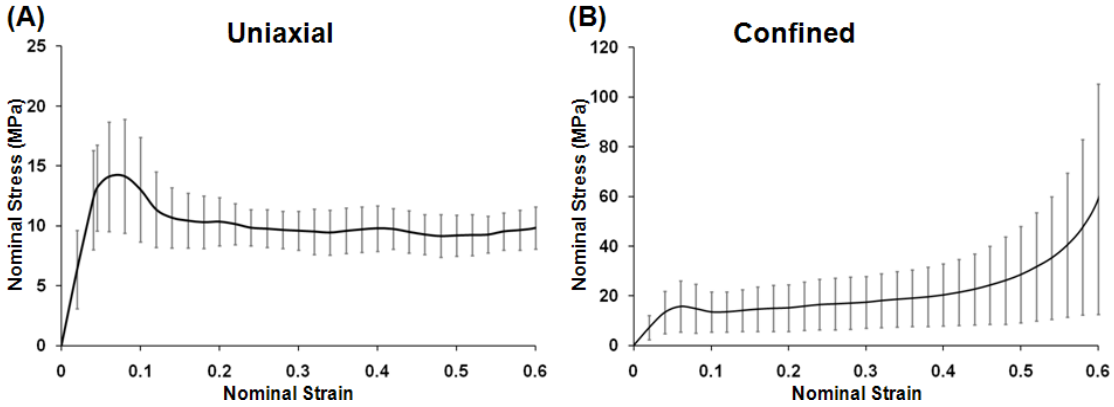

Fig. 6 - Bovine trabecular bone experimental results: (A) mean ± SD for uniaxial compression; (B) mean ± SD for confined compression.

Table 1 - Experimentally measured material properties for cellular polyurethane foam and bovine trabecular bone under uniaxial compression. Results are reported as mean ± SD (range).

	Young's Modulus, E (MPa)	**Yield Stress, σ_y (MPa)**	**Elastic Poisson's Ratio, v_e**	**Plastic Poisson's Ratio, v_p**
PU Foam (Grade 20)	141.3 ± 40.9 (76.4-165.9)	3.8 ± 0.7 (2.8-4.6)	0.20 ± 0.06 (0.14-0.28)	0.23 ± 0.08 (0.13-0.36)
BTB	381.7 ± 181.9 (168.5-798.4)	13.2 ± 3.6 (9.2-20.9)	0.16 ± 0.05 (0.12-0.2)	0.29 ± 0.20 (0.17-0.47)

Experimentally measured nominal stress-nominal strain plots for the uniaxial and confined compression testing of the cellular PU and the proximal tibial BTB are illustrated in Fig. 5 and Fig. 6 respectively. All experimental testing involved strain beyond the yield point and in all cases permanent plastic deformation was observed. The specimens undergo permanent plastic deformation with a very small amount of elastic recovery upon load removal. The elasto-plastic behaviour of cellular PU and BTB exhibit distinctive yielding. Material properties

experimentally measured for both specimen types (mean ± SD (range)) under uniaxial compression are shown in Table 1. The magnitudes of the mean measured values of E and σ_y for cellular PU under uniaxial compression are 141.3 ± 40.9 MPa and 3.8 ± 0.7 MPa respectively. Under uniaxial compression, the magnitudes of the mean E and σ_y for BTB are 381.7 ± 181.9 MPa and 13.2 ± 3.6 MPa respectively. Regarding the uniaxial compression data (Fig. 5(A), Fig. 6(A), Table 1), the cellular PU and BTB specimens show a similar nominal stress-nominal strain response. Under uniaxial compression the measured σ_y for BTB (13.2 MPa) is greater than the cellular PU (3.8 MPa) by a factor of 3.5. Also the measured E for BTB (381.7 MPa) is a factor of 2.7 greater than the cellular PU (141.3 MPa). A similar uniaxial compressive mean v_e is measured for cellular PU (0.20 ± 0.06) and BTB (0.16 ± 0.05). Despite quantitative differences measured for cellular PU and BTB, qualitatively similar inelastic deformation characteristics are observed. A plateau region of nearly constant stress is observed post-yield at ~3.5 MPa and ~10 MPa for the cellular PU and BTB respectively. This is followed by material densification occurring at ~50 % strain for the cellular PU. Regarding the confined compression results, the nominal stress (in the loading direction) exhibits distinctive yield behaviour for the cellular PU (Fig. 5(B)) and BTB (Fig. 6(B)). Most importantly, both specimen types exhibit a flat nominal stress-nominal strain curve following the initial yielding, resembling a perfect-plasticity nominal stress-nominal strain curve. An increase in nominal stress at higher strains occurs at ~40 % strain for both specimen types.

3.2 Material model

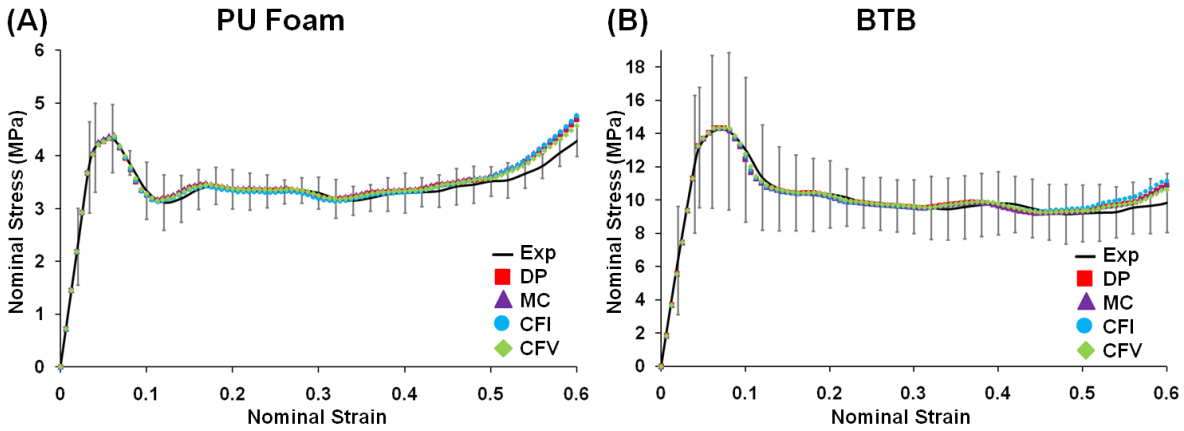

Fig. 7 - Uniaxial compression Drucker-Prager (DP), Mohr-Coulomb (MC), isotropic crushable foam (CFI), volumetric crushable foam (CFV) and experimental (mean ± SD) results: (A) cellular PU foam; (B) BTB.

The four aforementioned plasticity formulations (DP, MC, CFI and CFV) are calibrated to replicate the cellular PU and BTB experimental data for uniaxial compression as shown in Fig. 7. Each formulation is capable of capturing the inelastic behaviour under uniaxial compression conditions, including the yield, peak, plateau and densification.

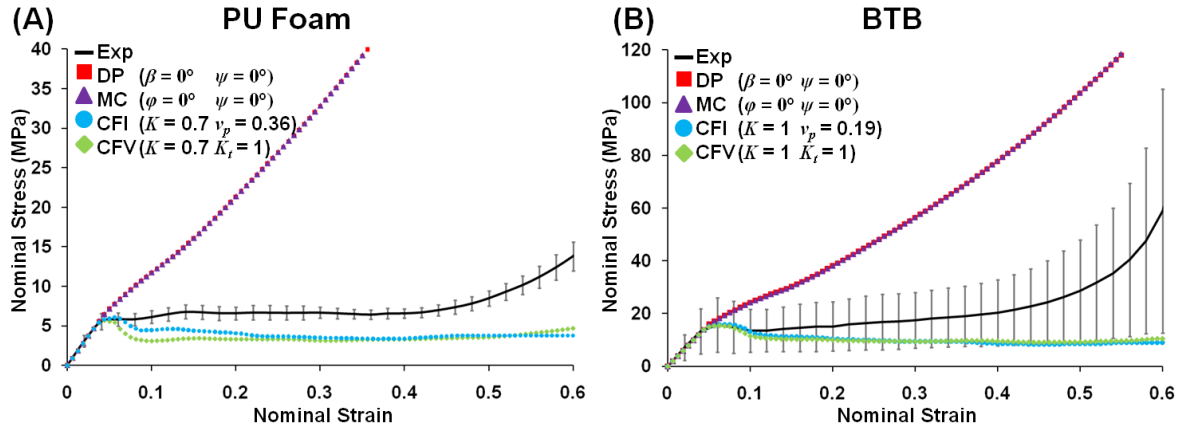

Fig. 8 - Confined compression Drucker-Prager (DP), Mohr-Coulomb (MC), isotropic crushable foam (CFI), volumetric crushable foam (CFV) and experimental (mean ± SD) results: (A) cellular PU foam; (B) BTB.

Next, using the material parameters calibrated from the uniaxial compression test, confined compression is simulated using the four plasticity formulations (Fig. 8). Firstly, it should be noted that the initial elastic response in confined compression is accurately simulated (for each model) using the mean experimentally measured E for both cellular PU and BTB and by performing a parametric study of v_e (Fig. 8, Table 1). A computed v_e of 0.28 for the cellular PU and 0.16 for the BTB respectively give a very good fit to our confined experimental data. These values lie in the range of the v_e reported in Table 1, measured using video extensometry. Next focusing on the plastic response under confined compression, it is shown in Fig. 8 that the DP and MC material models cannot replicate the experimental nominal stress-nominal strain data. For both the DP and MC models a friction angle = 0° and a dilations angle = 0° provide the closest match to the confined experimental results for both specimen types. In contrast to the DP and MC models, the CFI and CFV models accurately capture the initial yield behaviour of both the cellular PU and BTB under confined compression (Fig. 8). A best fit is obtained with a uniaxial to hydrostatic yield stress ratio of K = 0.7 for PU and K = 1 for BTB, illustrating the significant role played by pressure stress in the onset of plastic behaviour for both materials. Plateau behaviour is computed for both materials following initial yielding, similar to that observed experimentally, however, under predicting the experimental results. Predicted stresses lie within the experimental standard deviations for BTB up to a nominal strain of 0.42. For the CFI model K = 1 and v_p = 0.19 provides the best fit for BTB. This value of v_p falls within the experimentally measured range for BTB (Table 1). For the cellular PU K = 0.7 and v_p = 0.36 provides the best match. Again, v_p is within the measured range (Fig. 8(A), Table 1). While identical K values are determined for the CFI and CFV models, providing accurate initial yield predictions, the CFV model offers limited ability to calibrate peak stress under confined compression and lateral deformation under compression. In contrast, calibration of v_p in the CFI model allows for accurate simulation of peak stress and lateral deformation.

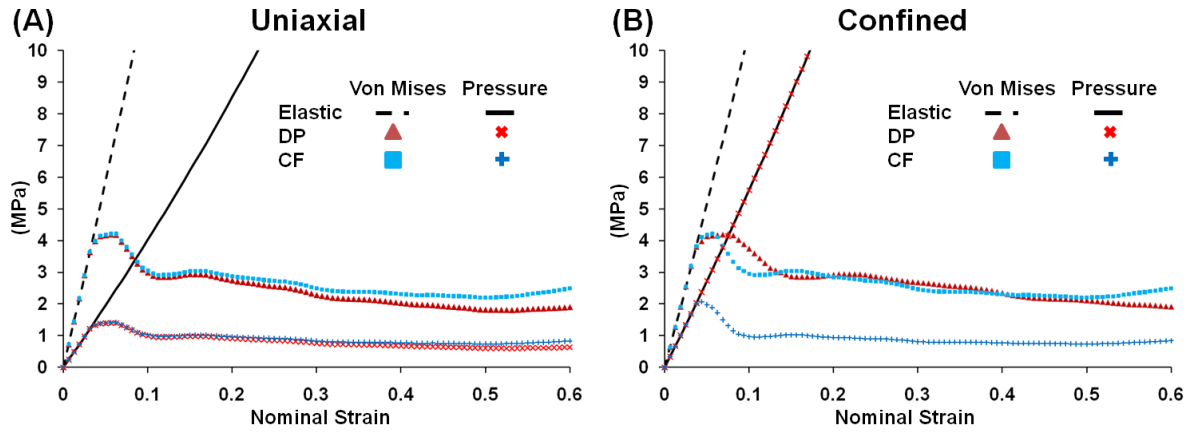

Fig. 9 - Schematic of the contribution of pressure stress and von Mises stress for an elastic, Drucker-Prager (DP) and crushable foam (CF) simulation: (A) a uniaxial compression test; (B) a confined compression test.

In order to further illustrate the fundamental differences between the predicted behaviour for linear yield surfaces (DP and MC models) and elliptical yield surfaces (CFI and CFV models), Fig. 9 plots the evolution of von Mises stress and pressure predicted for uniaxial (Fig. 9(A)) and confined (Fig. 9(B)) compression. In the case of uniaxial compression, there is only one non-zero stress component, which is equal to the von Mises stress. The pressure is at all times equal to one third of this stress, so no notable differences exist between the DP and crushable foam models. For confined compression, in addition to the stress component in the loading direction, lateral stress components also exist and the pressure is no longer simply given as $p = q/3$. As shown in Fig. 9(B), even though the von Mises stress follows a yield criterion, no pressure dependent yield is computed for the DP model, with the computed pressure being equal to the elastic solution. As a result, the nominal stress in the loading direction does not exhibit the required yield behaviour, as is evident from Fig. 9. In contrast, for the crushable foam models, both the von Mises stress and pressure stress follow a yield criterion, thus resulting in a pronounced yield in the predicted nominal stress.

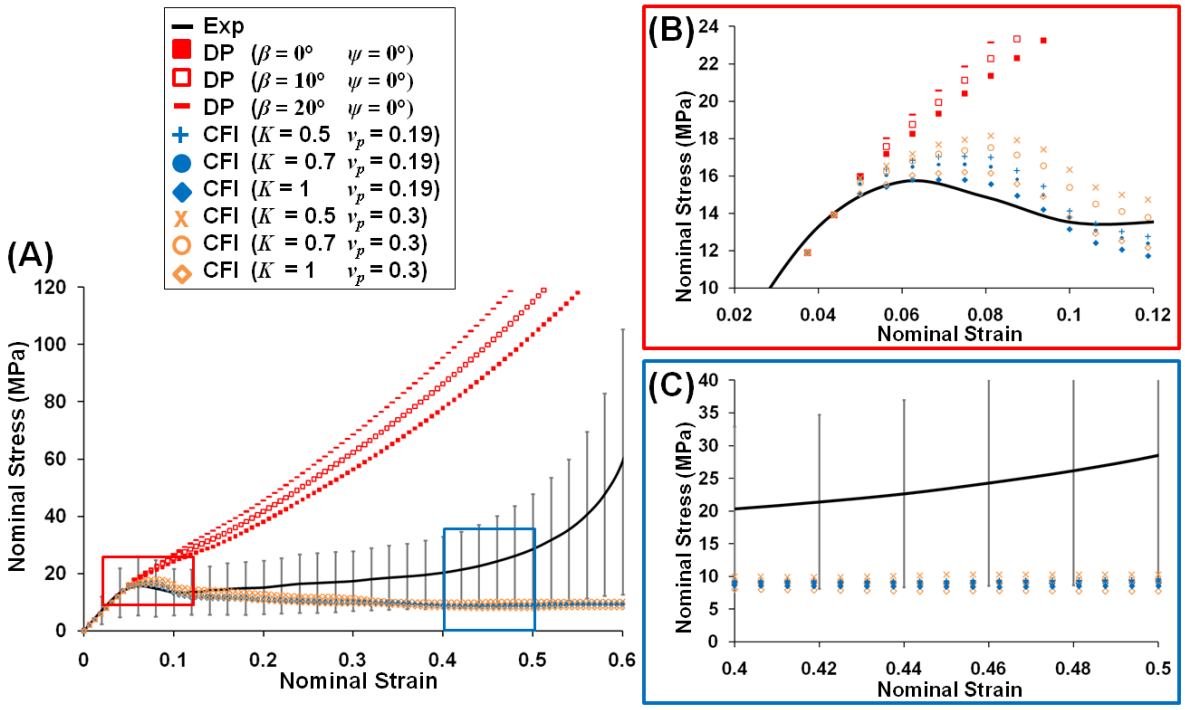

Fig. 10 - (A) Confined compression experimental BTB results (mean ± SD) and BTB parametric study results for the Drucker-Prager (DP) and isotropic crushable foam (CFI) material models; (B) Yield and peak stress behaviour; (C) Plateau stress behaviour for a nominal strain of 0.4 to 0.5.

To gain further insight, parametric studies are presented in Fig. 10 for the DP and CFI models for BTB. A range of v_p and K values are considered for the CFI model. As previously shown, $K = 1$ and $v_p = 0.19$ provides the best fit for the experimentally observed initial yield. A decrease in K (as shown for $K = 0.7$ and $K = 0.5$ in Fig. 10(A,B) results in a slightly over predicted yield stress and peak stress. A lower value of K reduces the pressure dependent yield, thus increasing the stress at which plasticity initiates. As expected, the v_p has no effect on the initial yield. Increasing the v_p (from 0.19 to 0.3) generally results in an increase in both the peak stress (Fig. 10(B)) and the plateau (Fig. 10(A,C)). It was not possible to accurately predict the plateau stress at high nominal strains (> 0.15) without significantly over predicting the initial yield and peak stresses. As previously noted, however, the CFI model provides the best prediction of experimental test data for PU and BTB. Also shown in Fig. 10 for the DP model, increasing the friction angle of the DP or MC models (from 0° to 20°) results in even more inaccurate predictions**,** as expected, with higher friction angles further delaying the onset of yield.

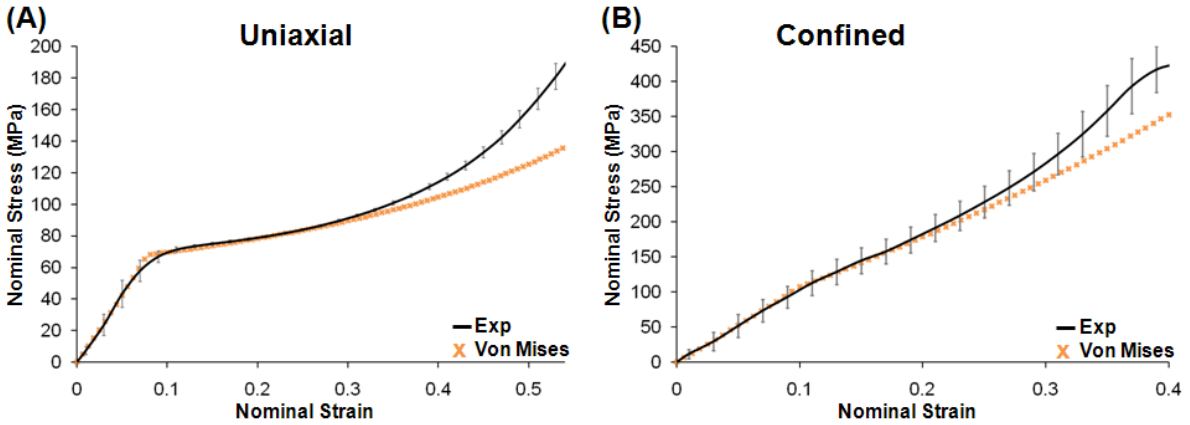

Fig. 11 - (A) Experimental and computational (von Mises plasticity) uniaxial compression testing results (mean ± SD) for grade 50 solid rigid PU foam. (B) Experimental and computational (von Mises plasticity) confined compression testing results (mean ± SD) for grade 50 solid rigid PU foam.

The experimental (mean ± SD) and computational (von Mises plasticity model) uniaxial and confined compression testing results for the solid PU are shown in Fig. 11. Under uniaxial compression, yield is followed by a plateau region and then densification, which is similar to the cellular PU and BTB (Fig. 5(A) and 6(A) respectively). No distinct yield is apparent under confined compression for the solid PU which is in stark contrast to the cellular PU and BTB (Fig. 5(B) and 6(B) respectively). The uniaxial and confined compressive behaviour of the solid PU is captured by a perfectly plastic von Mises plasticity model (Fig. 11), in which yielding is independent of hydrostatic stress. This simple model is equivalent to a DP model with a frication angle of 0°. Despite the yield curve in uniaxial compression, the solid PU does not yield in confined compression, where an increase in pressure leads to increased elastic strain, as illustrated in Fig. 9. Preliminary uniaxial compression testing of the cellular PU in the three loading directions showed no statistical difference *($p<0.05$)* for σ_y or at 40 % strain. No significant cellular PU anisotropy was evident from these macroscale results, providing justification for the use of isotropic constitutive models for these PU foams.

4. Discussion

The inelastic pressure dependent compressive behaviour of BTB is investigated through experimental and computational analysis. Two loading configurations are implemented, uniaxial and confined compression, providing two distinct loading paths in the *q*-*p* plane. Experimental results reveal distinctive yielding followed by a constant nominal stress plateau for both uniaxial and confined compression. Computational simulation of the experimental tests using the DP and MC plasticity models fails to capture the confined compression behaviour of BTB. The high pressure developed during confined compression does not result in plastic deformation using these formulations, and a near elastic response is computed. In contrast, crushable foam plasticity models provide accurate simulation of confined compression tests, with distinctive yield and plateau behaviour being predicted. The elliptical yield surfaces of these formulations in the *q*-*p* plane accurately characterise the plastic behaviour of BTB. It is also demonstrated that cellular PU exhibits similar pressure dependent yield behaviour, despite having a lower stiffness and strength than trabecular bone, supporting the use of cellular PU as a biomechanical test substitute material for trabecular bone applications involving multiaxial loading.

Several attempts have been made previously to calibrate constitutive plasticity models for cortical bone under different loading conditions. The DP and MC models have been successfully calibrated for cortical bone (Mercer et al., 2006; Tai et al., 2006; Mullins et al., 2009). Using the MC model for cortical bone Tai et al. (2006) calibrated a friction angle of 15°. Mullins et al. (2009) and Mercer et al. (2006) calibrated the DP model for cortical bone with values of (β = 46°, K_{DP} = 1, ψ = 0°) and (β = 43.5°, K_{DP} = 1) respectively. Few plasticity models have been calibrated for trabecular bone. Wang et al. (2008) calibrated the MC model with a friction angle of 12.9° for canine vertebral trabecular bone. However, this nanoindentation study probed individual trabeculae and is not reflective of the macroscale inelastic behaviour of the porous trabecular bone structure. To our knowledge the present study is the first attempt to characterise the pressure dependent yield behaviour of trabecular bone. We demonstrate that for DP and MC plasticity sufficient yielding is prevented at higher pressures in confined compression. In contrast, the crushable foam models better represent the inelastic behaviour of cellular PU and BTB, predicting a plateau region post yield for confined compression due to significant pressure dependent yielding. Results suggest that a ratio of uniaxial to hydrostatic yield stress K = 1 provides a good fit for BTB, with a slightly lower ratio being computed for cellular PU (K = 0.7), indicating the importance of modelling pressure dependent yield for both materials (K = 0 represents a standard von Mises type plasticity formulation). For the crushable foam models considered in the present study the computed plateau stress at high levels of deformation in the confined compression tests is lower than that observed experimentally. This suggests that a crushable foam plasticity model in which the ratio of uniaxial to pressure yield stress changes with plastic strain may provide further improvements in accuracy. The CFI and CFV plasticity models have previously been applied to cellular foams (Rizov et al., 2005; Flores-Johnson et al., 2008), however to our knowledge they have never been applied to trabecular bone.

Strain-based plasticity models that neglect pressure dependent yield, have been developed and implemented for trabecular bone (Cowin and He, 2005) and cortical bone (Natali et al., 2008). There are plausible reasons for adopting strain-based yield criterion for trabecular bone given the experimental evidence that within an anatomic site trabecular bone yield strains are more constant than the corresponding yield stresses and Young's

moduli site (Chang et al., 1999; Morgan and Keaveny, 2001). Based on the anisotropic elastic characterisation of trabecular bone by Van Rietbergen et al. (1996, 1998), Cowin and He, (2005) proposed a yield criterion based on a uniform yield stress, i.e. an anisotropic yield stress is determined from the elastic constants. A multiaxial strain-based criterion proposed by Natali et al. (2008) has been applied to cortical bone and uses an effective strain quantity to define a yield criterion. This effective strain is a strain-based version of the von Mises stress, so is constructed from the deviatoric strain tensor. It is important to note that, similar to von Mises plasticity, this yield criterion does not allow for any yielding due to volumetric strain (strain-based criterion) or hydrostatic stress (stress-based criterion). Based on the results of the present study under confined compression, we have demonstrated that yielding associated with hydrostatic stress or volumetric strain is an essential feature of the inelastic behaviour of trabecular bone. Based on the encouraging application of crushable foam models to trabecular bone in the current study, coupled with previous experimental evidence of consistent strain for trabecular bone within anatomic site, the authors suggest that future work should entail the development of a multiaxial strain-based yield criterion that includes yield due volumetric strain for trabecular bone. However further extensive multiaxial experimental tests under different q/p ratios will be required to develop such a yield criterion.

Solid PU and cellular PU are commonly used to synthesise trabecular bone for the biomechanical testing of implants (Agneskirchner et al., 2006; Poukalova et al., 2010; Cawley et al., 2011). An accurate representation of its elasto-plastic behaviour is essential in assessing its suitability as a test material substitute for trabecular bone for applications in which large deformation occurs (e.g. bone fracture, press-fit implantation in total joint arthroplasty). The cellular PU exhibits similar pressure dependent yield behaviour to BTB, despite this density foam having a lower Young's modulus and uniaxial yield stress than BTB. However, qualitatively similar elasto-plastic behaviour is observed for cellular PU and BTB with flat plateau regions evident under confined compression. In stark contrast to the cellular PU and BTB, the solid PU does not display pressure dependent yield in confined compression due to its near solid structure. A simple von Mises perfectly plastic material model, in which yielding is independent of hydrostatic stress, predicts the solid PU uniaxial and confined data very well. The results of the present study demonstrate the influence of the cellular PU structure in replicating the inelastic behaviour of trabecular bone under confined compression.

Previous studies have primarily relied on uniaxial testing to characterise elastic properties of trabecular bone (Goldstein, 1987; Røhl et al., 1991; Kopperdahl and Keaveny, 1998) and PU trabecular bone analogue (Thompson et al., 2003; Johnson and Keller, 2008; Patel et al., 2008; Calvert et al., 2010). In terms of elastic properties, the mean Young's modulus of grade 20 cellular PU measured in this study (141.3 MPa) is very close to the value of 137 MPa reported by the manufacturer and in previous studies (Thompson et al., 2003; Patel et al., 2008). Regarding trabecular bone, previous studies reported a similar mean (485 ± 333 MPa) and range (1.4 - 552 MPa) of Young's modulus values for human proximal tibial trabecular bone (Goldstein, 1987; Røhl et al., 1991; Kopperdahl and Keaveny, 1998). Our BTB yield stress of 13.2 ± 3.6 MPa is comparable with reported values by Morgan and Keaveny (2001) for the human proximal tibia (5.83 ± 3.42 MPa) and femoral neck (17.45 ± 6.15 MPa). Our measured BTB elastic Poisson's ratio is within the range reported for the human proximal tibia of 0.07 - 0.65 (Klever et al., 1985). The large experimental standard deviations reported are in line with previous uniaxial compressive testing of trabecular bone (Røhl et al., 1991; Kopperdahl and Keaveny, 1998; Morgan and Keaveny, 2001). Larger standard deviations exist for BTB than PU which is attributed to the

inherent inconsistent properties of trabecular bone. The BTB specimens were taken from a single bovine tibia from the same anatomical location (proximal tibia) and were tested along their principal loading axis. Despite this, variation in the structural confirmation of specimens is likely to have attributed to the scatter evident in the experimental results. Morgan and Keaveny (2001) performed on-axis uniaxial compression testing on trabecular bone specimens from the vertebrae, proximal tibia, femoral neck and greater trochanter and measured a large scatter in data for the different anatomical locations and within anatomical site. Material properties measured from uniaxial compressive testing of proximal tibial trabecular specimens taken from various locations can vary by up to two orders of magnitude (Goldstein et al., 1983). In the present study, testing multiple specimens from the proximal tibial accounted for the inherent biological heterogeneity of trabecular bone within a single anatomic site. Although the cellular PU and BTB have a similar cellular structure, there are some distinct differences between the two materials. In addition to the lack of bone marrow, closed cell PU foams lack the open cell structure of trabecular bone. Despite such differences, qualitatively similar stress-strain curves are evident for the two cellular materials under both loading modes.

Very few studies have considered the confined compression behaviour of trabecular bone (Linde and Hvid, 1989; Charlebois et al., 2010b) despite the fact that this loading mode is physiologically relevant, given that *in-vivo* trabecular bone is confined by a stiff cortical shell. The studies of Gibson (2005) and Szivek et al. (1993) reported the three phase uniaxial stress-strain behaviour of trabecular bone but did not implement confined compression testing. Charlebois et al. (2010b) performed an investigation of the role of morphological measures determined from micro computed tomography (μCT) scans, namely volume fraction and a fabric tensor, in the elastic and post yield behaviour of trabecular bone under uniaxial and confined conditions. An earlier study Linde and Hvid (1989) investigated the elastic behaviour of trabecular bone using both uniaxial and confined compression testing, however plasticity was not considered. Due to the lack of experimental data, the confined compression results could not be compared to previous studies.

Like cellular foams, the failure mechanisms of trabecular bone are highly influenced by its cellular structure. The combination of rod and plate like trabeculae as well as the horizontal and vertical composition vary with anatomic site and are affected by numerous factors. Gibson (1985) proposed three failure modes for cellular solids: elastic buckling; plastic hinging; brittle fracture. Under progressive compressive loading cellular materials absorb large amounts of energy and the trabeculae undergo a combination of these failure modes simultaneously. While slender rod like trabeculae may be buckling, stouter rod or plate like trabeculae may be yielding. Micro-compression tests have predicted the failure of rod like trabeculae to occur due to bending and buckling which is followed by trabeculae collapse when overloaded (Muller et al., 1998). Bending or buckling was not predicted for plate like trabeculae and instantaneous failure occurred (Muller et al., 1998). An experimental and numerical investigation by Deshpande and Fleck (2000) showed a pressure dependent yield in the yield surface of open cell and closed cell metallic foams. Using the crushable foam model developed by Deshpande and Fleck (2000) to represent the crushing and buckling behaviour of cellular foams, the present study uncovered similar pressure dependent yield behaviour for BTB and cellular PU in confined compression.

The intrinsic material properties and structural composition of trabeculae play a fundamental role in trabecular bone failure mechanisms. Macroscale inelastic continuum material models have been proposed that represent the trabecular bone morphology (Zysset and Curnier, 1996; Zysset and Rincon-Kohli, 2006; Rincon-Kohli and

Zysset, 2009; Charlebois et al., 2010a) where fabric-based tensors and volume fraction describe the material heterogeneity and anisotropy respectively. Such models include information on the structural conformation of the trabeculae from the analysis of 3D reconstructions. However, the importance of pressure dependent yield has not been considered. Micro-architecture based FE models, based on high-resolution images such as μCT data, explicitly represent individual trabecular geometries (McDonnell et al.; Niebur et al., 2000; Niebur et al., 2002; Bayraktar et al., 2004; Harrison and McHugh, 2010; Guillén et al., 2011). Niebur et al. (2002) performed bi-axial testing and investigated the influence of the trabecular structure on yield. Similar to other studies (Niebur et al., 2000; Bayraktar et al., 2004; Guillén et al., 2011), a bi-linear asymmetric material model that neglects pressure dependent yield was used to describe the yield behaviour. These bi-linear models offer limited capability of matching the post-yield behaviour as they rely on a reduction of the material stiffness post-yield to 5 % when the critical principal strain is exceeded, an assumption that is based on post-yield testing of cortical bone specimens. The microscale pressure dependent yield behaviour of trabecular bone could not be exposed due to the constant *q/p* ratio for all simulations. Such micro-structural based FE models require considerable effort in relation to mesh generation and computational expense which limits their use for macroscale trabecular bone applications. However, the present continuum approach provides a phenomenological representation of the mechanical response due to the buckling and crushing of trabeculae that does not depend on the structural conformation of the material. In addition to the uniaxial testing already performed, further multiaxial testing in confined compression is required to phenomenologically capture the relationship between trabecular bone micro-architecture and multiaxial plastic deformation. Such testing as well as high-resolution imaging of trabecular specimens would allow for the development of more sophisticated continuum models that incorporate micro-structural descriptors.

Trabecular bone has an aligned composite porous micro structure and is both inhomogeneous and anisotropic (Townsend et al., 1975; Williams and Lewis, 1982; Hodgskinson and Currey, 1990). Solely on-axis uniaxial and confined compression testing was performed for BTB therefore the anisotropy of the trabecular specimens could not be determined. A significant limitation of the present study is that trabecular bone is modelled as an isotropic material. The current study took a significant step in uncovering the pressure dependent yield behaviour of trabecular bone at the macroscale. We demonstrate that crushable foam plasticity models with elliptical yield surfaces in the *p-q* plane capture this behaviour reasonably well. Although not tested in the present study, it is expected that a similar pressure dependent yield should occur regardless of the direction of loading, following from the fact that pressure is a stress invariant. However an extensive series of uniaxial, multiaxial and confined compression testing must be performed on trabecular bone to uncover the manner in which the ratio of uniaxial to pressure dependent yield should vary as a function of the material anisotropy. Pressure increase under confined compression is a function of Poisson's ratio, which will depend on the loading direction for an anisotropic material. Follow on studies should involve the extension of the phenomenological CFI and CFV models to include additional features such as material anisotropy and trabecular architecture.

A number of limitations and sources of error should be noted for the present study. The accuracy of the experimental testing directly influences the results obtained. As trabecular bone is naturally confined by cortical bone, confined compression testing was performed as an approximation of the in-vivo situation. Purely hydrostatic loading would have been desirable and may be investigated in a future study. BTB was used over

cadaveric specimens to its similarity to human trabecular bone. The focus of this study was on the inelastic behaviour of trabecular bone and it is expected that similar pressure dependent yield behaviour would be evident for cadaveric specimens taken from various anatomical locations. Standard experimental errors due to friction, damage and machine compliance have been previously reported for compression testing of trabecular bone and should be noted in the present study also (Linde and Hvid, 1989; Odgaard and Linde, 1991; Linde et al., 1992; Keaveny et al., 1993a;1993b). Although unavoidable for the test methods employed damage artifacts due to specimen machining interrupt the natural trabecular network have also been previously reported (Odgaard and Linde, 1991; Linde et al., 1992; Keaveny et al., 1997). Additionally frictional artifacts at the compression platens represent a further source of test error (Brown and Ferguson, 1980; Odgaard and Linde, 1991). Errors due to specimen alignment with the platens, pre-existing specimen damage and off-axis specimens would have also induced approximations in the experimental results. Due care was taken during the preparation, alignment and testing of all specimens to minimise any possible errors. No creep recovery was observed following load removal, indicating that viscoelasticity is not a dominant mechanism. All testing was performed at a constant strain rate, eliminating the introduction of any strain rate sensitivity in the yield behaviour. Although not investigated, strain rate effects have been shown to influence on trabecular bone compressive behaviour (Galante et al., 1970; Linde et al., 1991). Further experimental testing and application of the CFI and CFV material models to trabecular bone loading at various strain rates is desirable. Damage models were not investigated but may be able to capture the inelastic behaviour observed experimentally for BTB. We suggest that, similar to the yield function in the CF plasticity models, an appropriate damage model should include a damage component driven by hydrostatic stress.

Whole bone fracture, the implantation of press-fit devices and subsidence of prostheses involve multiaxial loading and inelastic deformation that lead to significant hydrostatic stresses due to naturally confined nature of trabecular bone. The findings of the present study will allow for improved prediction of trabecular bone plasticity in such a complex environment.

5. Conclusions

In order to investigate the inelastic behaviour of trabecular bone both uniaxial and confined compression were performed, representing two different loading paths in the *q-p* plane and elucidating for the first time the pressure dependent yield behaviour. An assessment of established plasticity constitutive formulations revealed that trabecular bone is best represented by an elliptical yield surface in the *q-p* plane, characteristic of crushable foam plasticity. In contrast, plasticity models typically used for cortical bone, such as the DP or MC formulations are unsuitable for trabecular bone, given that a pressure increase leads to a reduced plastic deformation in such models. We also demonstrate that cellular PU synthetic bone analogue exhibits similar pressure dependent yield behaviour to trabecular bone, despite having a lower strength and stiffness. In contrast, solid PU does not exhibit pressure dependent yield in confined compression due to its near solid structure. The enhanced understanding of the inelastic behaviour of trabecular bone provided by this study will allow for more realistic simulation of the performance of implant devices. Specifically, ongoing work entails further experimental testing and model development to assess the inelastic deformation of trabecular bone during the implantation of press-fit total arthroplasty components.

Appendix - Constitutive Formulations

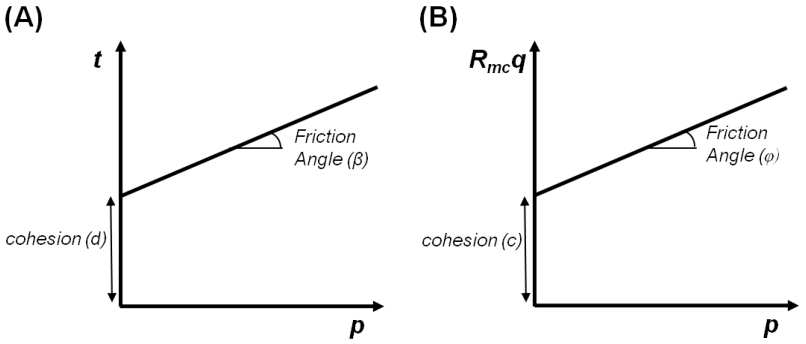

Fig. A.1 – (A) Drucker-Prager yield criterion. (B) Mohr-Coulomb yield criterion.

Drucker-Prager Constitutive Model

The yield criterion for the modified DP model is given by: $F = t - ptan\beta - d = 0$

Where $t = \frac{q}{2}\left[1 + \frac{1}{K_{DP}} - \left(1 - \frac{1}{K_{DP}}\right)\left(\frac{r}{q}\right)^3\right]$

The flow potential is given by: $G = t - ptan\psi$

Where t is the DP deviatoric stress measure, β is the friction angle of the material, d is the material cohesion, K_{DP} is the flow stress ratio in tension and compression, r is the third invariant of deviatoric stress and ψ is the dilation angle (Drucker and Prager, 1951).

Mohr-Coulomb Constitutive Model

The yield criterion for the MC model is given by: $F = R_{mc}q - pTan\varphi - c = 0$

The flow potential is given by: $G = \sqrt{(\epsilon c|_0 tan\psi)^2 + (R_{mw}q)^2} - pTan\psi$

Where R_{mc} is the MC deviatoric stress measure, φ is the friction angle of the material, c is the cohesion yield stress, ϵ is the meridional eccentricity, $c|_0$ is the initial cohesion yield stress and ψ is the dilation angle.

Acknowledgements

The authors would like to thank: Pat Kelly for technical assistance; Brady's Abattoir in Athenry for bovine specimens; the College of Engineering and Informatics for providing a studentship for NK.

References

Adam, C. J. and Swain, M. V., 2011. The effect of friction on indenter force and pile-up in numerical simulations of bone nanoindentation. J. Mech. Behav. Biomed. Mater. 4, 1554-1558.

Agneskirchner, J., Freiling, D., Hurschler, C. and Lobenhoffer, P., 2006. Primary stability of four different implants for opening wedge high tibial osteotomy. Knee Surg. Sports Traumatol. Arthrosc. 14, 291-300.

ASTM (2008). Standard Specification for Rigid Polyurethane Foam for Use as a Standard Material for Testing Orthopaedic Devices and Instruments. ASTM F1839-01. ASTM. Pennsylvania.

Bayraktar, H. H., Gupta, A., Kwon, R. Y., Papadopoulos, P. and Keaveny, T. M., 2004. The Modified Super-Ellipsoid Yield Criterion for Human Trabecular Bone. J Biomech Eng. 126, 677-684.

Bayraktar, H. H. and Keaveny, T. M., 2004. Mechanisms of uniformity of yield strains for trabecular bone. J Biomech. 37, 1671-1678.

Bessho, M., Ohnishi, I., Matsuyama, J., Matsumoto, T., Imai, K. and Nakamura, K., 2007. Prediction of strength and strain of the proximal femur by a CT-based finite element method. J Biomech. 40, 1745-1753.

Brown, T. D. and Ferguson, A. B., 1980. Mechanical Property Distributions in the Cancellous Bone of the Human Proximal Femur. Acta Orthop. 51, 429-437.

Calvert, K. L., Trumble, K. P., Webster, T. J. and Kirkpatrick, L. A., 2010. Characterization of commercial rigid polyurethane foams used as bone analogs for implant testing. J Mater Sci: Mater Med. 21, 1453-1461.
Carnelli, D., Gastaldi, D., Sassi, V., Contro, R., Ortiz, C. and Vena, P., 2010. A Finite Element Model for Direction-Dependent Mechanical Response to Nanoindentation of Cortical Bone Allowing for Anisotropic Post-Yield Behavior of the Tissue. J Biomech Eng. 132, 1-10.
Carnelli, D., Lucchini, R., Ponzoni, M., Contro, R. and Vena, P., 2011. Nanoindentation testing and finite element simulations of cortical bone allowing for anisotropic elastic and inelastic mechanical response. J Biomech. 44, 1852-1858.
Cawley, D. T., Kelly, N., Simpkin, A., Shannon, F. J. and McGarry, J. P., 2011. Full and surface tibial cementation in total knee arthroplasty: A biomechanical investigation of stress distribution and remodeling in the tibia. Clin Biomech. In Press,
Chang, W. C. W., Christensen, T. M., Pinilla, T. P. and Keaveny, T. M., 1999. Uniaxial yield strains for bovine trabecular bone are isotropic and asymmetric. J Orthop Res. 17, 582-585.
Charlebois, M., Jirasek, M. and Zysset, P. K., 2010a. A nonlocal constitutive model for trabecular bone softening in compression. Biomech Model Mechanobiol. 9, 597-611.
Charlebois, M., Pretterklieber, M. and Zysset, P. K., 2010b. The Role of Fabric in the Large Strain Compressive Behavior of Human Trabecular Bone. J Biomech Eng. 132, 1-10.
Cowin, S. C. and He, Q. C., 2005. Tensile and compressive stress yield criteria for cancellous bone. J Biomech. 38, 141-144.
Deshpande, V. S. and Fleck, N. A., 2000. Isotropic constitutive models for metallic foams. J. Mech. Phys. Solids. 48, 1253-1283.
Drucker, D. C. and Prager, W. (1951). Soil mechanics and plastic analysis or limit design. Brown University. Division of Applied, Mathematics United States. Office of Naval, Research, Division of Applied Mathematics, Brown University.
Flores-Johnson, E. A., Li, Q. M. and Mines, R. A. W., 2008. Degradation of elastic modulus of progressively crushable foams in uniaxial compression. J Cell Plast. 44, 415.
Galante, J., Rostoker, W. and Ray, R. D., 1970. Physical properties of trabecular bone. Calcif. Tissue Int. 5, 236-246.
Gibson, L. J., 1985. The mechanical behaviour of cancellous bone. J Biomech. 18, 317-328.
Gibson, L. J., 2005. Biomechanics of cellular solids. J Biomech. 38, 377-399.
Goldstein, S. A., 1987. The mechanical properties of trabecular bone: dependence on anatomic location and function. J Biomech. 20, 1055-1061.
Goldstein, S. A., Wilson, D. L., Sonstegard, D. A. and Matthews, L. S., 1983. The mechanical properties of human tibial trabecular bone as a function of metaphyseal location. J Biomech. 16, 965-969.
Guillén, T., Zhang, Q. H., Tozzi, G., Ohrndorf, A., Christ, H. J. and Tong, J., 2011. Compressive behaviour of bovine cancellous bone and bone analogous materials, microCT characterisation and FE analysis. J. Mech. Behav. Biomed. Mater. 4, 1452-1461.
Harrison, N. and McHugh, P., 2010. Comparison of trabecular bone behavior in core and whole bone samples using high-resolution modeling of a vertebral body. Biomech Model Mechanobiol. 9, 469-480.
Harrison, N. M., McDonnell, P. F., O'Mahoney, D. C., Kennedy, O. D., O'Brien, F. J. and McHugh, P. E., 2008. Heterogeneous linear elastic trabecular bone modelling using micro-CT attenuation data and experimentally measured heterogeneous tissue properties. J Biomech. 41, 2589-2596.
Hodgskinson, R. and Currey, J. D., 1990. The effect of variation in structure on the Young's modulus of cancellous bone: a comparison of human and non human material. Proc. Inst. Mech. Eng. 204, 115-121.
Johnson, A. E. and Keller, T. S., 2008. Mechanical properties of open-cell foam synthetic thoracic vertebrae. J Mater Sci: Mater Med. 19, 1317-1323.
Keaveny, T. M., Borchers, R. E., Gibson, L. J. and Hayes, W. C., 1993a. Theoretical analysis of the experimental artifact in trabecular bone compressive modulus. J Biomech. 26, 599-607.
Keaveny, T. M., Borchers, R. E., Gibson, L. J. and Hayes, W. C., 1993b. Trabecular bone modulus and strength can depend on specimen geometry. J Biomech. 26, 991-1000.
Keaveny, T. M., Morgan, E. F., Niebur, G. L. and Yeh, O. C., 2001. Biomechanics of trabecular bone. Annu. Rev. Biomed. Eng. 3, 307-333.
Keaveny, T. M., Pinilla, T. P., Crawford, P. R., Kopperdahl, D. L. and Lou, A., 1997. Systematic and random errors in compression testing of trabecular bone. J Orthop Res. 15, 101-110.
Keaveny, T. M., Wachtel, E. F. and Kopperdahl, D. L., 1999. Mechanical behavior of human trabecular bone after overloading. J Orthop Res. 17, 346-353.
Kelly, N. and McGarry, J. P. 2011. Experimental and computational characterization of the elasto-plastic properties of a synthetic polyurethane trabecular bone analogue 57th Annual Meeting of the Orthopaedic Research Society, Long Beach, California.
Keyak, J. H., 2001. Improved prediction of proximal femoral fracture load using nonlinear finite element models. Med Eng Phys. 23, 165-173.
Keyak, J. H. and Rossi, S. A., 2000. Prediction of femoral fracture load using finite element models: an examination of stress- and strain-based failure theories. J Biomech. 33, 209-214.
Klever, F. J., Klumpert, R., Grootenboer, H. J., van Campen, D. H. and Pauly, T., 1985. Global mechanical properties of trabecular bone: experimental determination and prediction from a structural model. J Biomech. 18, 522-522.
Kopperdahl, D. L. and Keaveny, T. M., 1998. Yield strain behavior of trabecular bone. J Biomech. 31, 601-608.
Linde, F., 1994. Elastic and viscoelastic properties of trabecular bone by a compression testing approach. Dan. Med. Bull. 41, 119.

Linde, F. and Hvid, I., 1989. The effect of constraint on the mechanical behaviour of trabecular bone specimens. J Biomech. 22, 485-490.
Linde, F., Hvid, I. and Madsen, F., 1992. The effect of specimen geometry on the mechanical behaviour of trabecular bone specimens. J Biomech. 25, 359-368.
Linde, F., Norgaard, P., Hvid, I., Odgaard, A. and Soballe, K., 1991. Mechanical properties of trabecular bone. Dependency on strain rate. J Biomech. 24, 803-809.
Lotz, J. C., Cheal, E. J. and Hayes, W. C., 1991. Fracture prediction for the proximal femur using finite element models: part I—linear analysis. J Biomech Eng. 113, 353.
Mc Donnell, P., Harrison, N., Liebschner, M. A. K. and Mc Hugh, P. E., 2009. Simulation of vertebral trabecular bone loss using voxel finite element analysis. J Biomech. 42, 2789-2796.
McDonnell, P., Harrison, N. and McHugh, P. E., Investigation of the failure behaviour of vertebral trabecular architectures under uni-axial compression and wedge action loading conditions. 32, 569-576.
Mercer, C., He, M. Y., Wang, R. and Evans, A. G., 2006. Mechanisms governing the inelastic deformation of cortical bone and application to trabecular bone. Acta Biomater. 2, 59-68.
Moore, T. L. A. and Gibson, L. J., 2002a. Microdamage accumulation in bovine trabecular bone in uniaxial compression. 124, 63.
Moore, T. L. A. and Gibson, L. J., 2002b. Microdamage Accumulation in Bovine Trabecular Bone in Uniaxial Compression. J Biomech Eng. 124, 63-71.
Morgan, E. F., Bayraktar, H. H. and Keaveny, T. M., 2003. Trabecular bone modulus-density relationships depend on anatomic site. J Biomech. 36, 897-904.
Morgan, E. F. and Keaveny, T. M., 2001. Dependence of yield strain of human trabecular bone on anatomic site. J Biomech. 34, 569-577.
Muller, R., Gerber, S. C. and Hayes, W. C., 1998. Micro-compression: a novel technique for the nondestructive assessment of local bone failure. Technol Health Care. 6, 433-444.
Mullins, L. P., Bruzzi, M. S. and McHugh, P. E., 2009. Calibration of a constitutive model for the post-yield behaviour of cortical bone. J. Mech. Behav. Biomed. Mater. 2, 460-470.
Natali, A. N., Carniel, E. L. and Pavan, P. G., 2008. Constitutive modelling of inelastic behaviour of cortical bone. 30, 905-912.
Neilsen, M. K., Krieg, R. D. and Schreyer, H. L., 1995. A constitutive theory for rigid polyurethane foam. Polym Eng Sci. 35, 387-394.
Niebur, G. L., Feldstein, M. J. and Keaveny, T. M., 2002. Biaxial Failure Behavior of Bovine Tibial Trabecular Bone. J Biomech Eng. 124, 699-705.
Niebur, G. L., Feldstein, M. J., Yuen, J. C., Chen, T. J. and Keaveny, T. M., 2000. High-resolution finite element models with tissue strength asymmetry accurately predict failure of trabecular bone. J Biomech. 33, 1575-1583.
Odgaard, A. and Linde, F., 1991. The underestimation of Young's modulus in compressive testing of cancellous bone specimens. J Biomech. 24, 691-698.
Patel, P. S. D., Shepherd, D. E. T. and Hukins, D. W. L., 2008. Compressive properties of commercially available polyurethane foams as mechanical models for osteoporotic human cancellous bone. BMC Musculoskelet Disord. 9, 137.
Poukalova, M., Yakacki, C. M., Guldberg, R. E., Lin, A., Saing, M., Gillogly, S. D., et al., 2010. Pullout strength of suture anchors: Effect of mechanical properties of trabecular bone. J Biomech. 43, 1138-1145.
Rincon-Kohli, L. and Zysset, P., 2009. Multi-axial mechanical properties of human trabecular bone. Biomech Model Mechanobiol. 8, 195-208.
Rizov, V., Shipsha, A. and Zenkert, D., 2005. Indentation study of foam core sandwich composite panels. Comp Struct. 69, 95-102.
Røhl, L., Larsen, E., Linde, F., Odgaard, A. and Jørgensen, J., 1991. Tensile and compressive properties of cancellous bone. J Biomech. 24, 1143-1149.
Szivek, J. A., Thomas, M. and Benjamin, J. B., 1993. Technical note. Characterization of a synthetic foam as a model for human cancellous bone. J Appl Biomater. 4, 269-272.
Tai, K., Ulm, F.-J. and Ortiz, C., 2006. Nanogranular Origins of the Strength of Bone. Nano Lett. 6, 2520-2525.
Taylor, M., Tanner, K. E. and Freeman, M. A. R., 1998. Finite element analysis of the implanted proximal tibia: a relationship between the initial cancellous bone stresses and implant migration. J Biomech. 31, 303-310.
Thompson, M. S., McCarthy, I. D., Lidgren, L. and Ryd, L., 2003. Compressive and Shear Properties of Commercially Available Polyurethane Foams. J Biomech Eng. 125, 732-734.
Townsend, P. R., Raux, P., Rose, R. M., Miegel, R. E. and Radin, E. L., 1975. The distribution and anisotropy of the stiffness of cancellous bone in the human patella. J Biomech. 8, 363-364.
Turner, C. H., 1989. Yield Behavior of Bovine Cancellous Bone. J Biomech Eng. 111, 256-260.
Van Rietbergen, B., Odgaard, A., Kabel, J. and Huiskes, R., 1996. Direct mechanics assessment of elastic symmetries and properties of trabecular bone architecture. J Biomech. 29, 1653-1657.
Van Rietbergen, B., Odgaard, A., Kabel, J. and Huiskes, R., 1998. Relationships between bone morphology and bone elastic properties can be accurately quantified using high resolution computer reconstructions. J Orthop Res. 16, 23-28.
Wang, X., Allen, M. R., Burr, D. B., Lavernia, E. J., Jeremic, B. and Fyhrie, D. P., 2008. Identification of material parameters based on Mohr-Coulomb failure criterion for bisphosphonate treated canine vertebral cancellous bone. Bone. 43, 775-780.
Williams, J. L. and Lewis, J. L., 1982. Properties and an anisotropic model of cancellous bone from the proximal tibial epiphysis. J Biom Eng. 104, 50.

Zysset, P. and Rincon-Kohli, L., 2006. An alternative fabric-based yield and failure criterion for trabecular bone, in: Holzapfel, G. A. and Ogden, R. W. (Eds.), Mechanics of Biological Tissue. Springer, pp. 457-470.
Zysset, P. K. and Curnier, A., 1996. A 3D damage model for trabecular bone based on fabric tensors. J Biomech. 29, 1549-1558.